



STRUCTURAL SCIENCE  
CRYSTAL ENGINEERING  
MATERIALS

Volume 74 (2018)

**Supporting information for article:**

**Accurate and precise lattice parameters of H<sub>2</sub>O and D<sub>2</sub>O ice I<sub>h</sub> between 1.6 and 270 K from high-resolution time-of-flight neutron powder diffraction data**

**A. Dominic Fortes**

# Electronic Supplementary Text and Figures

Accurate and precise lattice parameters of H<sub>2</sub>O and D<sub>2</sub>O ice Ih between 1.6 and 270 K from high-resolution time-of-flight neutron powder diffraction data.

A. Dominic Fortes,<sup>1</sup>

<sup>1</sup>ISIS Facility, STFC Rutherford Appleton Laboratory, Harwell Science and Innovation Campus, Chilton, Didcot, Oxfordshire, OX11 0QX, U.K.

Corresponding author email [dominic.fortes@stfc.ac.uk](mailto:dominic.fortes@stfc.ac.uk)

## CONTENTS

### **1. Use of infrared thermography to evaluate thermal gradients in the samples.**

Figure S1: Photograph of the embedded sensor used to determine true sample temperatures.

Figure S2: Thermal image of the slab can and exposed sample during warming and control.

Figure S3: Contrast stretched thermal image of the exposed sample at 340 K.

### **2. Additional supplementary figures and tables**

Figure S4: Comparison of the ice Bragg peak shapes with selected instrumental standards.

Figure S5: Comparison of FWHM for ice and silicon Bragg peaks.

Figure S6: Multi-plot showing the transformation of ice I<sub>SD</sub> ice Ih on HRPD.

Figure S7: Comparison of diffraction data for three independently synthesised ice specimens.

Figure S8: Lattice parameters of D<sub>2</sub>O ice Ih referenced to their 5 K values.

Figure S9: Comparison of the lattice parameters of H<sub>2</sub>O and D<sub>2</sub>O ice Ih.

Figure S10: Comparison of the *c/a* ratios of H<sub>2</sub>O and D<sub>2</sub>O ice Ih.

Figure S11: Comparison of measured and model phonon densities of states.

Figure S12: Comparison of LaPlaca & Post's raw *a*-axis data with Haltenorth's.

Figure S13: Plot of the logged sample temperatures after insertion in the cryostat.

Table S1: Lattice parameters of H<sub>2</sub>O ice Ih as a function of temperature.

Table S2: Lattice parameters of D<sub>2</sub>O ice Ih as a function of temperature.

Table S3: List of all published determinations of the density of H<sub>2</sub>O ice Ih.

### **3. List of all cited references with titles.**

# Electronic Supplementary Text and Figures

## 1. Use of infrared thermography to evaluate thermal gradients in the samples.

As described in the main text, and shown in Figure S1, a slab can was fitted with a RhFe resistance thermometer inside the sample cavity (introduced through the back window). The purpose of this was to measure the temperature difference between the centre of the sample and that measured by the RhFe sensor that is routinely inserted into the aluminium frame of the sample holder. As the thermal diffusivity of the sample (particularly in its powdered state) is typically much smaller than that of the aluminium frame, there will be a lag between the sample temperature that requires a period of equilibration once the temperature of the holder reaches and controls at the set point.

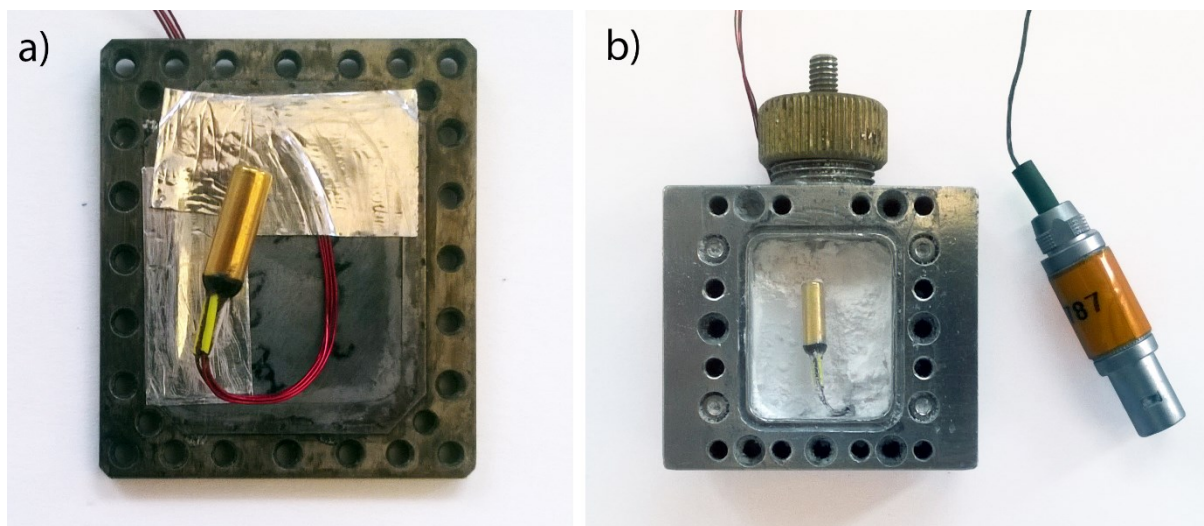


Figure S1. (a) The internal sensor wired through a standard vanadium window. The package is 10 mm long and 3.1 mm in diameter. (b) The assembled can, half filled with MgO powder.

Since it is considerably more convenient to load, and since I wished to carry out *ex situ* thermal imaging at and above room temperature, I chose to perform these tests with MgO powder instead of ice. MgO is a reasonable proxy in terms of its thermal diffusivity for a mixture of ice and silicon. At 295 K the thermal diffusivity,  $\alpha$ , of MgO is  $15.5 \times 10^{-6} \text{ m}^2 \text{ s}^{-1}$  (Hoffmeister, 2014). A crude estimate of the thermal diffusivity of the ice-silicon mixture may be obtained from scaling by their volume abundances; thus for an estimated 75:25 mix of ice ( $15.4 \times 10^{-7} \text{ m}^2 \text{ s}^{-1}$ : e.g., Slack, 1980) and silicon ( $8.5 \times 10^{-5} \text{ m}^2 \text{ s}^{-1}$ : Glassenbrenner & Slack, 1964) by volume, I find  $\alpha \approx 22 \times 10^{-6} \text{ m}^2 \text{ s}^{-1}$ . These quantities are, of course, representative of the bulk crystalline solid and will be considerably smaller in the powder.

## Electronic Supplementary Text and Figures

For snow with a bulk density comparable to that of my powdered ice specimens ( $\sim 0.7 \text{ g cm}^{-3}$ ), the formulas given by Sakatume & Seki (1978) and Fukusako (1990) indicate a thermal *conductivity*  $\sim 0.75$  of the bulk crystalline value. Hence, the thermal diffusivity of MgO is probably very similar to a mixture of ice and silicon, at least at higher temperatures. It is evident, furthermore, that adding silicon does far more than ensure accuracy of the lattice parameters, it also ensures faster equilibration and hence more accurate temperatures by increasing the thermal diffusivity of the sample.

Both the frame temperature and the embedded sample temperature were logged with the MgO sample mounted in a cryostat as a variety of different thermal cycles were performed. These included free cooling (i.e., following the CCR down in temperature without internal heating), controlled cooling (with PID-controlled halts every 20 K), and several cycles of controlled warming.

These data reveal a near uniform offset between the frame and sample temperatures when the system is at room temperature and not being actively heated, as well as when the system is being actively controlled below room temperature, of  $110 \pm 140 \text{ mK}$ .

Since the two resistance thermometers only sample the temperature at two locations, infrared thermography was used to identify any significant spatial temperature variations, resulting from packing inhomogeneity for example. Mid-range thermal imaging equipment allows images with a spatial resolution of better than 1 mm per pixel to be obtained from a distance of 30 cm and with a precision of  $< 0.1 \text{ K}$ . Inevitably, imaging must be done outside the cryostat and with one of the vanadium windows removed so that the sample may be viewed directly. Consequently, tests were done in the open air to evaluate the cell performance on heating and cooling in the range 295 – 340 K, both with and without one of the windows attached. Unsurprisingly, thermal control is very poor with one window removed, and so images could only be acquired during brief exposures of the sample.

Images were acquired with a FLIR E8 camera, supplied by Red Current Ltd., UK. The camera captures images on an uncooled micro-bolometer with 320 x 240 pixels, through a fixed lens of 45 x 34° field of view, and with a stated precision of 0.06 K.

Figure S2 shows representative thermal images collected during the warming from 295 to 340 K (a) and (b) and once the 340 K setpoint was reached and both the frame and embedded sensors were in equilibrium (c). Images were post-processed in FLIR Tools; an emissivity of 0.78 was applied in order to obtain accurate temperatures on the sample.

## Electronic Supplementary Text and Figures

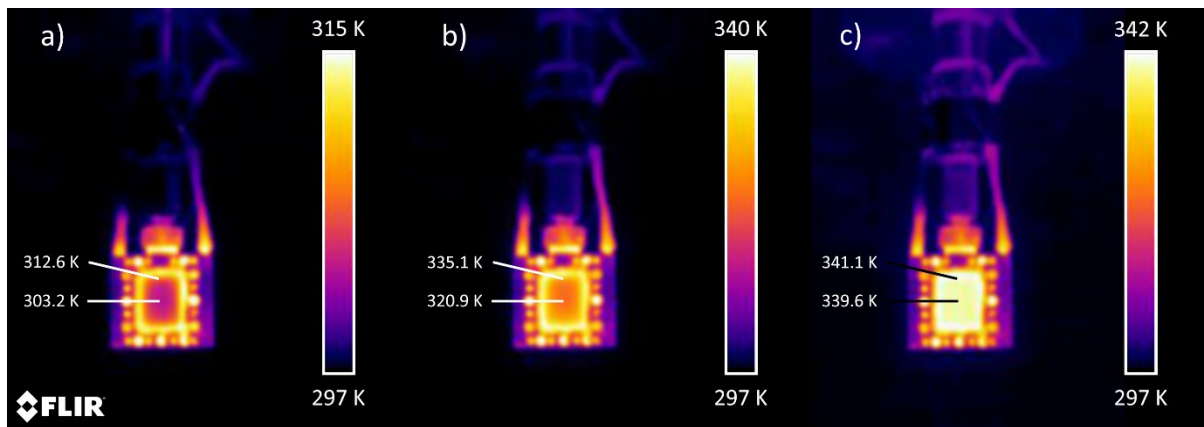


Figure S2. Thermal images, captured using a FLIR E8 camera, of the heated sample holder and the exposed sample. The cartridge heater is on the right and the RhFe sensor mounted in the frame is on the left of each image. Since proper heating of the sample requires the window to be attached, this was removed momentarily for the images to be captured.

Thermal gradients of 10 – 15 K between the edge and the centre of the sample are typical of the heating phase, and accurately reflect the magnitude of the thermal lags seen in the resistance thermometers. Once controlling at 340 K, however, the gradients observed are similar to 1 K.

Closer examination of ‘hot’ spots around the edge of the sample (Figure S3) shows that they are spatially correlated with loose and disturbed powder (compare the gouges in the visible-light image with the warm regions in the thermal image). This disturbed powder is the result of applying a soft brush during loading to clean up excess powder and then removal of the window to capture thermal images.

Where the powder is well packed in the middle of the exposed face, thermal gradients are small. In particular, the oval region where the relative neutron flux is > 85 % of its peak value (indicated on the intensity map in Fig. S3) has a temperature of  $340.0 \pm 0.2$  K.

To summarise, thermal imaging of well consolidated specimens reinforces the observations from the embedded resistance thermometer that there no significant thermal gradients in the region sampled by the most intense portion of the incident neutron beam.

## Electronic Supplementary Text and Figures

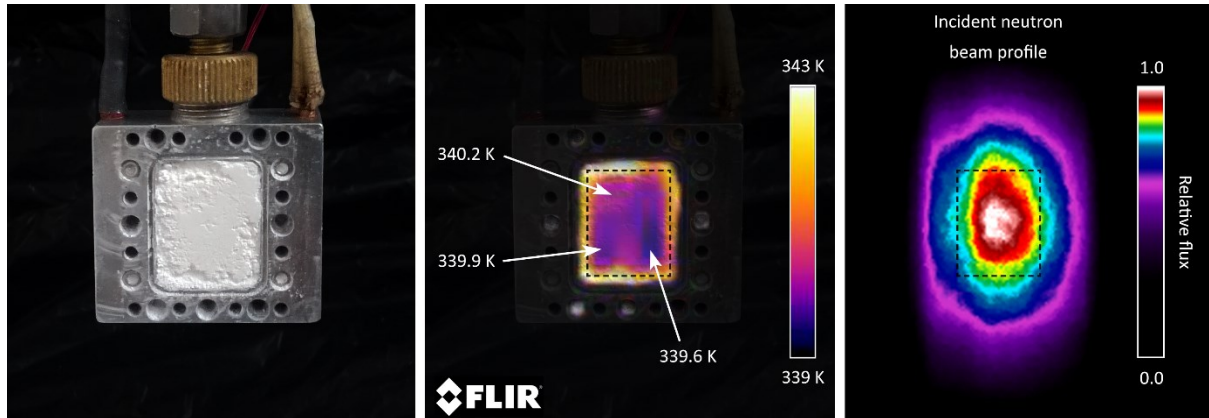


Figure S3. The central thermal image is from Figure S2c, with the thermal contrast stretched to highlight variations across the surface of the exposed sample. Spatial resolution is 0.6 mm per pixel in this image acquired from a distance of < 25 cm. The thermal image is superimposed on a visible-light image of the sample can (also shown on the left for clarity, with a pixel resolution of 0.06 mm). The black dashed line shows the region of the sample that is actually illuminated by the neutron beam. The panel on the right shows a direct image of the actual neutron flux distribution in HRPD's standard 30 – 130 ms time-of-flight and with the standard vertical and horizontal jaw gaps equal to 20 and 15 mm, respectively (Neutron camera provided courtesy of Dr Craig Bull, ISIS).

# Electronic Supplementary Text and Figures

## 2. Additional supplementary plots

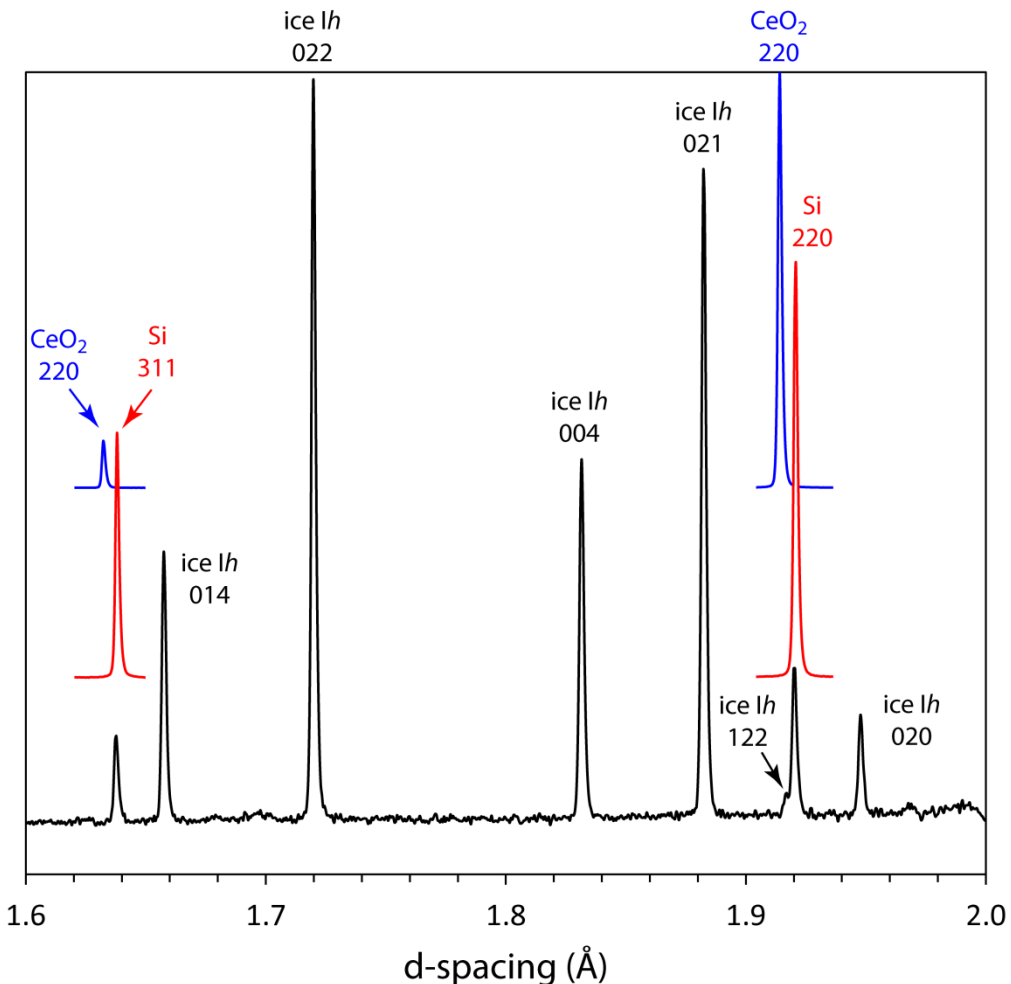


Figure S4: Segment of powder diffraction data collected from D<sub>2</sub>O ice Ih at 2 K (D<sub>2</sub>O series 2), measured in HRPD's backscattering detectors. Shown for comparison in red and blue are calibration measurements collected from NIST silicon and from a ceria pellet (note that only two reflections from each are present in this range), the latter being used on HRPD as a line-shape standard to define the instrumental resolution. This clearly shows that the ice Bragg peaks are of comparable width to the sharp line standards and exhibit no *hkl*-dependent broadening or asymmetry.

## Electronic Supplementary Text and Figures

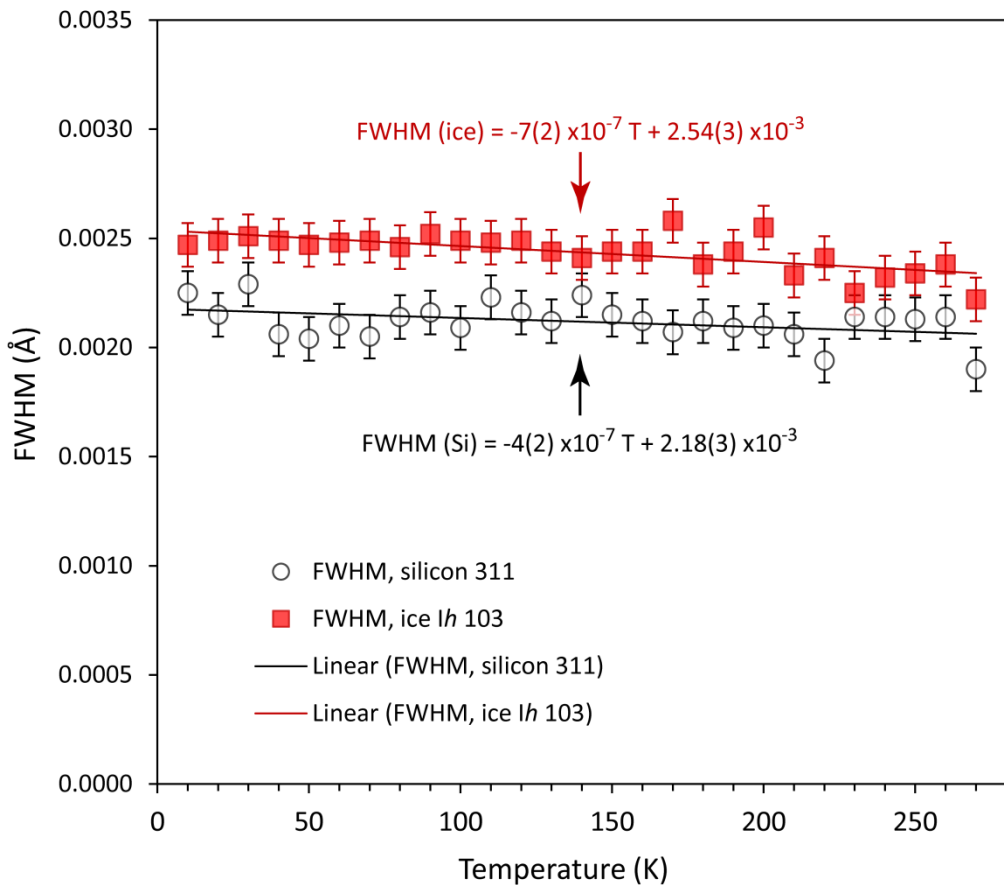


Figure S5: Extracted full width at half maximum (FWHM) for Bragg peaks from ice and silicon in the backscattering data for D<sub>2</sub>O series 1. Note that the FWHM of the ice reflection is only slightly larger than that of the silicon reflection, both exhibit essentially the same temperature dependence and neither exhibits any anomalous kinks or changes in slope. This is good evidence that the ice does not preserve any significant strain from the cooling used to prepare it, does not undergo any obvious relaxation (such as might occur by annealing out of defects) and shows no correlation with anomalies observed in the axial ratios.

## Electronic Supplementary Text and Figures

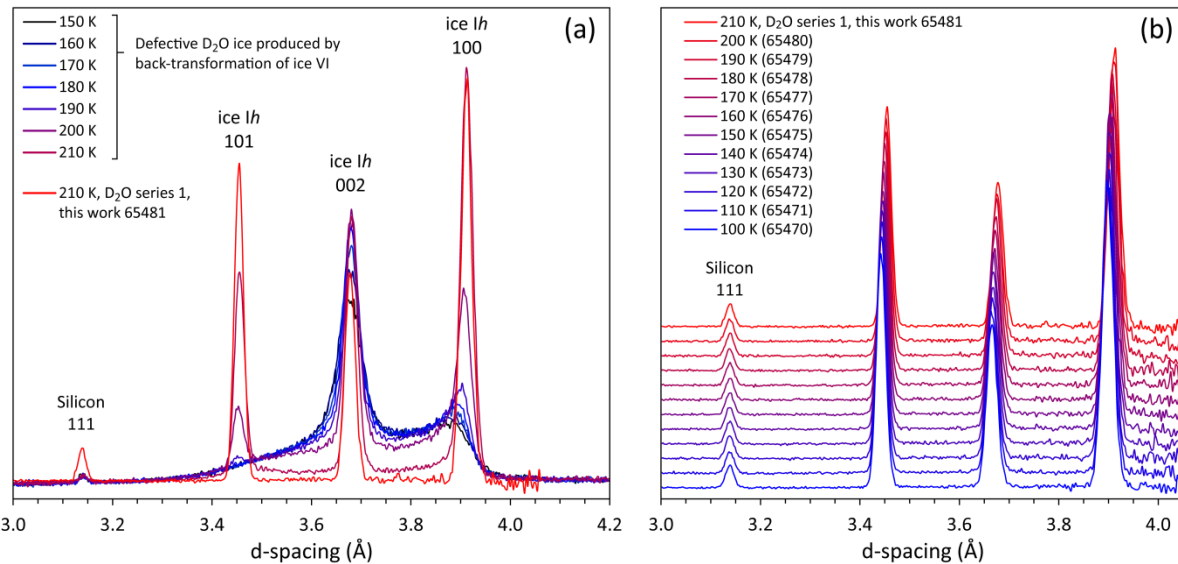


Figure S6: (a) Multiplot showing powder diffraction data acquired in HRPD's 90° detector banks (thus at lower resolution than the backscattering data shown elsewhere) during the back-transformation of recovered D<sub>2</sub>O ice VI. The data, beginning at 150 K, reveal the formation of high-cubicity stacking-defective ice that anneals on warming to form progressively less defective material. At 210 K, where this experiment was ended, the ice is substantially hexagonal in nature and the manifestation of some residual cubicity is apparent only in a slight broadening of 002 and in the meniscuses of diffuse scattering between the Bragg peaks. For comparison, a dataset measured at 210 K in this work is overlaid, which shows that the peaks are sharper, 101 is more intense and the diffuse scattering is absent. This shows that the ice measured in this work, from which all of the analysis follows, was wholly or substantially hexagonal in character and did not possess stacking faults at the level where they would be detectable. (b) Multiplot depicting the diffraction data from this work (D<sub>2</sub>O series 1) collected on warming from 100 – 210 K; the uppermost diffraction pattern is thus the same one shown in the panel on the left. Apart from a shift to longer d-spacings due to thermal expansion, the Bragg peaks exhibit no variation in intensity or width.

The ice I<sub>SD</sub> powder data are reproduced with the kind permission of Prof. Ian Wood, University College London.

## Electronic Supplementary Text and Figures

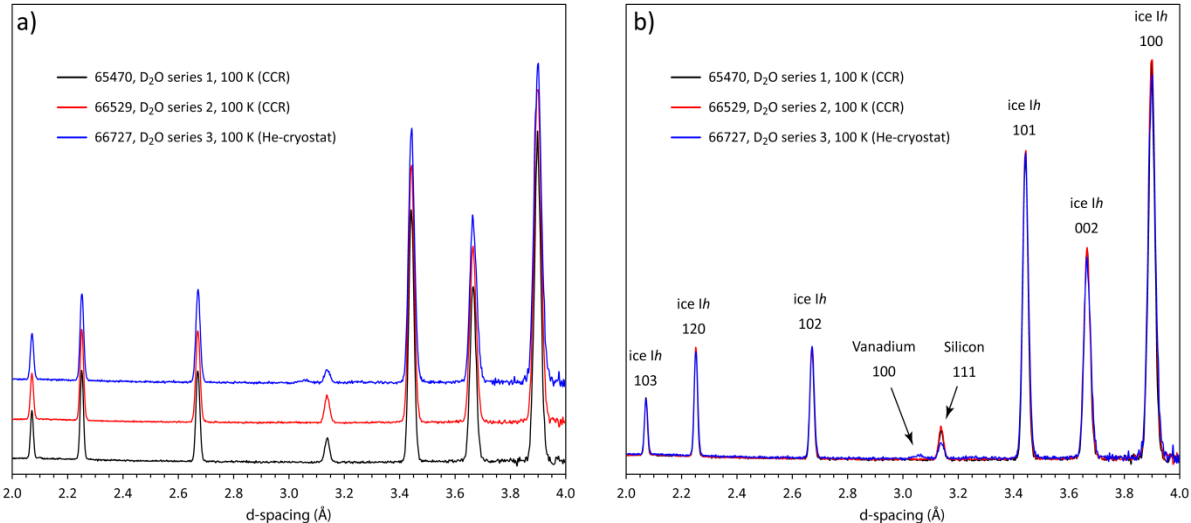


Figure S7: Data measured at 100 K in HRPD's 90° detectors from the three different D<sub>2</sub>O ice Ih specimens, shown separated on the left and collapsed on the right. This reinforces the observation from Figure S6 that the peaks are sharp and have no residual diffuse intensity and further illustrates that the same is true of all three D<sub>2</sub>O samples. Indeed the peak widths, intensities and backgrounds of all three specimens are nearly identical. Small differences in the data are restricted to the silicon 111 peak (due simply to different amounts of silicon powder being mixed with the ice) and a very weak vanadium peak in the specimen measured using a helium cryostat due to the presence of additional V-foil windows compared with the closed-cycle refrigerator.

## Electronic Supplementary Text and Figures

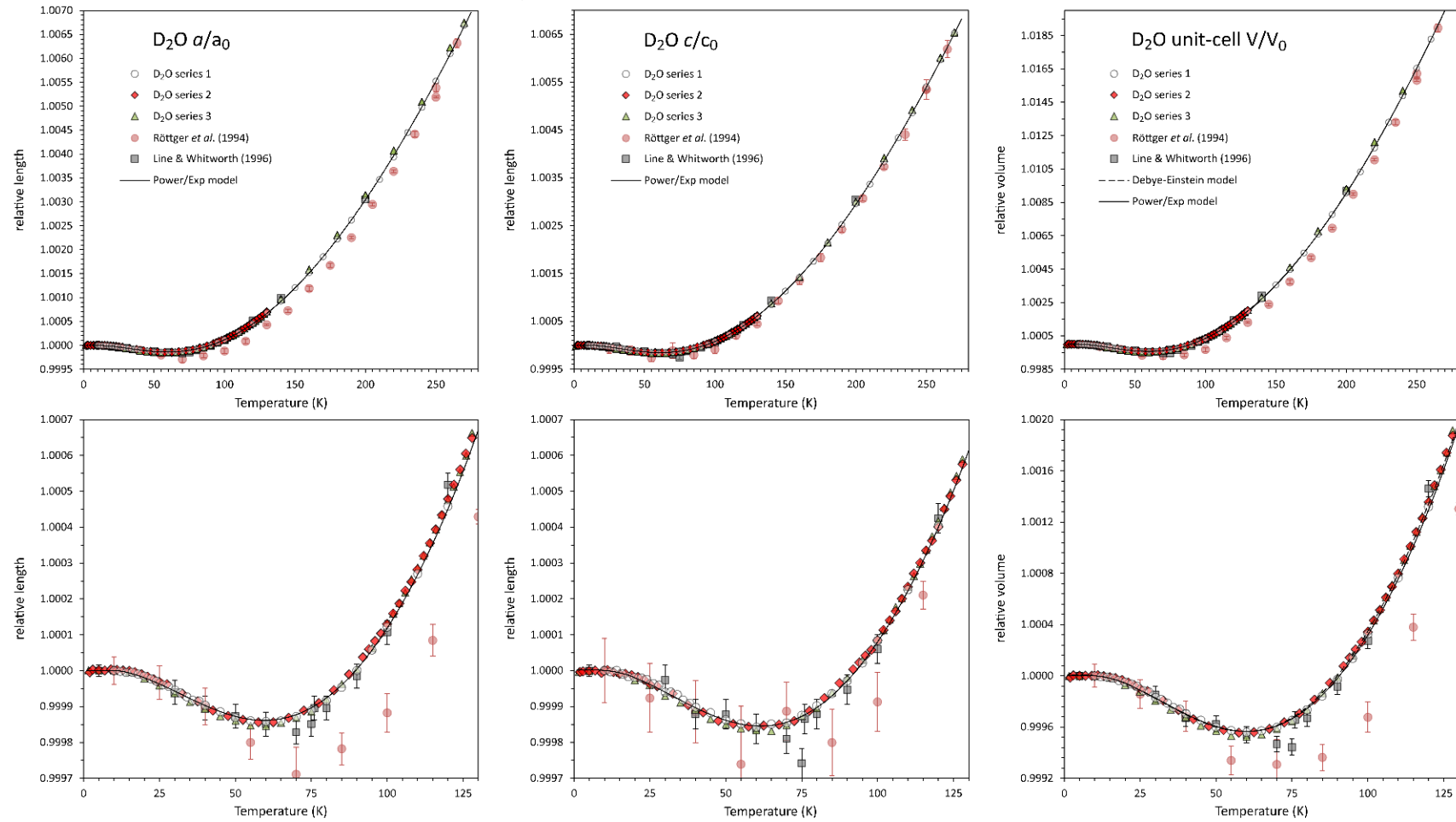


Figure S8: Lattice parameters of  $\text{D}_2\text{O}$  ice  $\text{Ih}$  referenced to their 10 K values (since this was only low-T datum in common between all three samples), although described as  $a/a_0$  etc. There is very good agreement between the relative values of the three new series, as well as with the dataset measured on HRPD twenty-two years ago (Line & Whitworth, 1996). Agreement with Röttger *et al.* (1994, 2012) is poorer.

## Electronic Supplementary Text and Figures

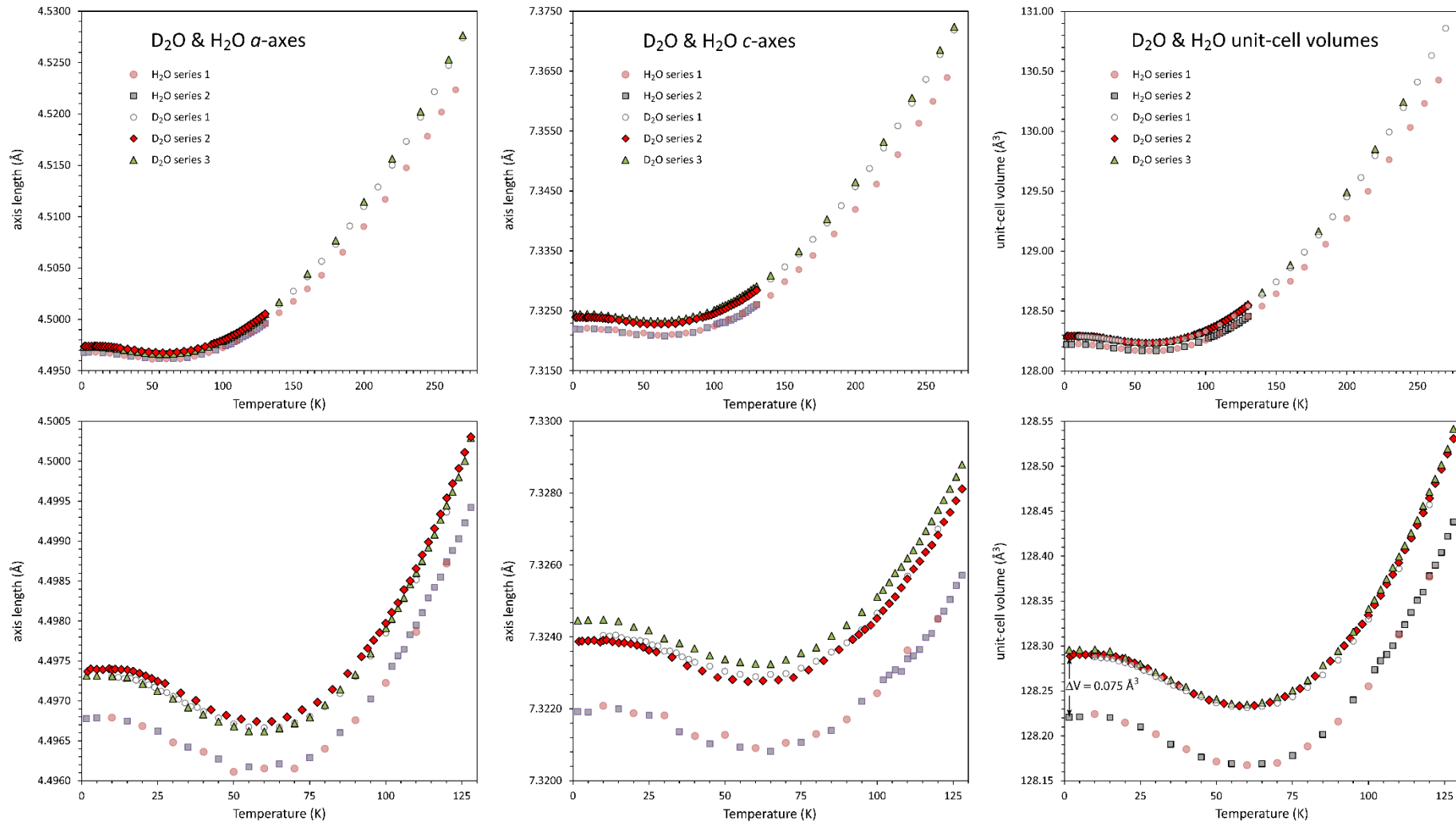


Figure S9: Comparison of the absolute lattice parameters of  $\text{H}_2\text{O}$  and  $\text{D}_2\text{O}$  ice  $Ih$ .

## Electronic Supplementary Text and Figures

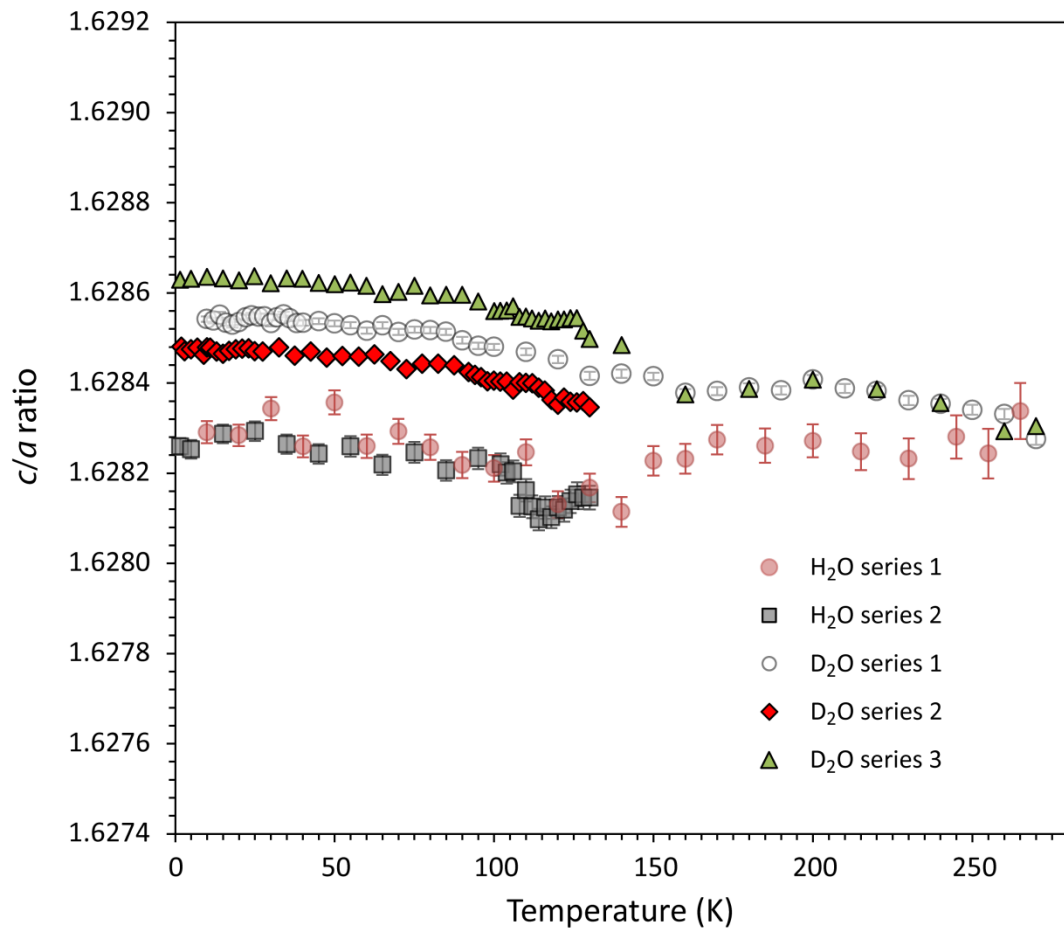


Figure S10: Comparison of the  $c/a$  ratios of  $\text{H}_2\text{O}$  and  $\text{D}_2\text{O}$  ice  $\text{Ih}$ .

## Electronic Supplementary Text and Figures

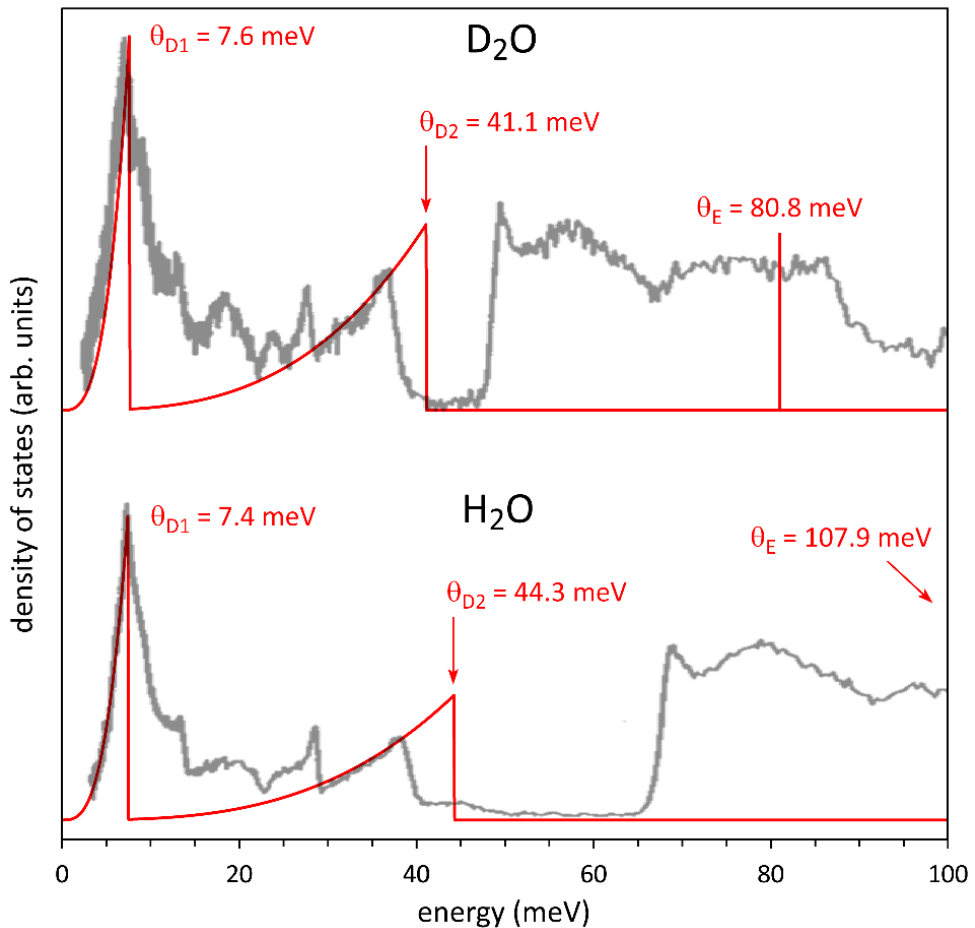


Figure S11: Comparison of measured and model phonon densities of states. The grey lines show the vibrational densities of states obtained by inelastic neutron spectroscopy (Li, 1996). The solid red lines a representative of the double-Debye + Einstein oscillator model used to fit the volume thermal expansion. The two Debye terms at lower frequencies,  $\theta_{D1}$  and  $\theta_{D2}$ , correspond rather well with the gross features of the measured spectrum, particularly in relation to the transverse acoustic peak at  $\sim 7$  meV that controls the negative expansion at low temperatures. Conversely, the delta function that represents the Einstein term ( $\theta_E$ ) is a much poorer (and entirely *ad hoc*) representation of the higher frequency portion of the spectrum.

# Electronic Supplementary Text and Figures

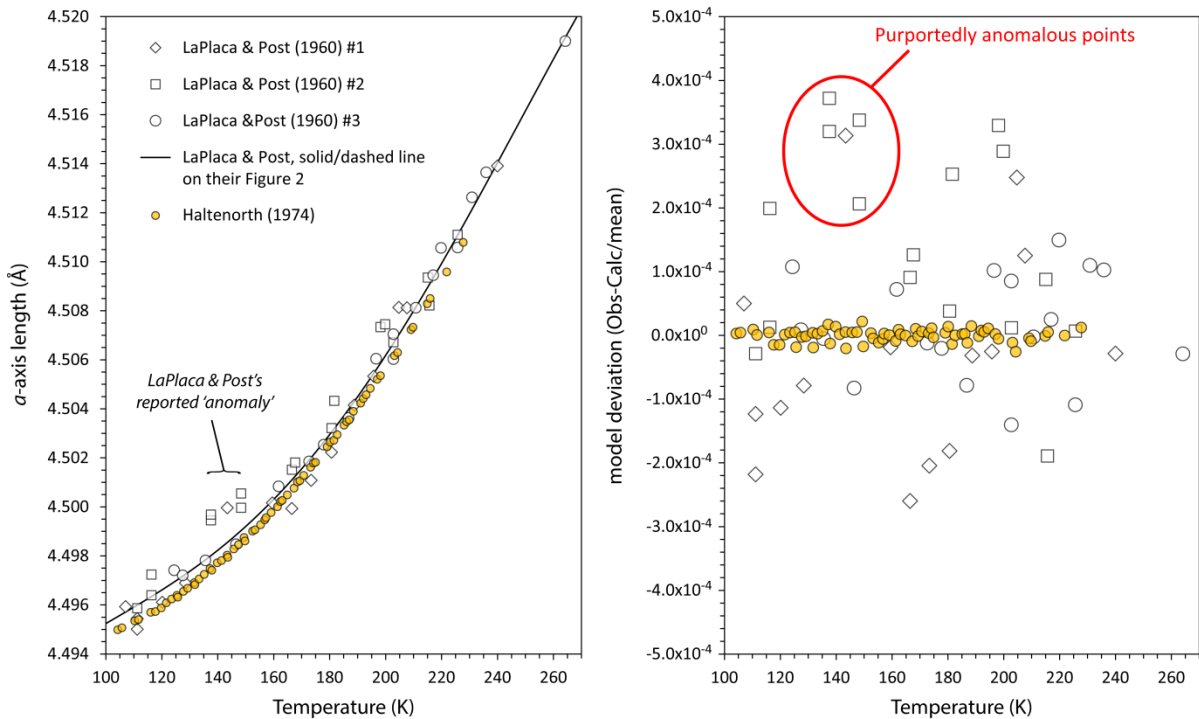


Figure S12: Left, plot of ‘raw’  $a$ -axis lengths from the paper of LaPlaca & Post (1960) and the thesis of Haltenorth (1974). The symbols from LaPlaca & Post’s work correspond to the three reported data series that they measured over a period of several months and the solid line corresponds with the solid/dashed line in their Figure 2. Highlighted are the points that are described as a reproducible plateau or anomaly.

One the right is shown the relative deviation of the symbols from the solid line in LaPlaca & Post (1960); it is thus apparent that the anomalous points are not statistically significantly different from the other measurements and that the purported anomaly is not real. The greater *perceived* deviation of the points around 140 K compared with those around 200 K in the left-hand figure is probably due to the difference in slope of the trend line, resulting in an optical illusion.

For comparison, the scatter in Haltenorth’s data about a fitted third-order polynomial are an order of magnitude smaller, being a few  $\times 10^{-5}$ . As Haltenorth states at multiple points in the text of his thesis, there is no  $a$ -axis anomaly comparable with that reported by LaPlaca and Post.

## Electronic Supplementary Text and Figures

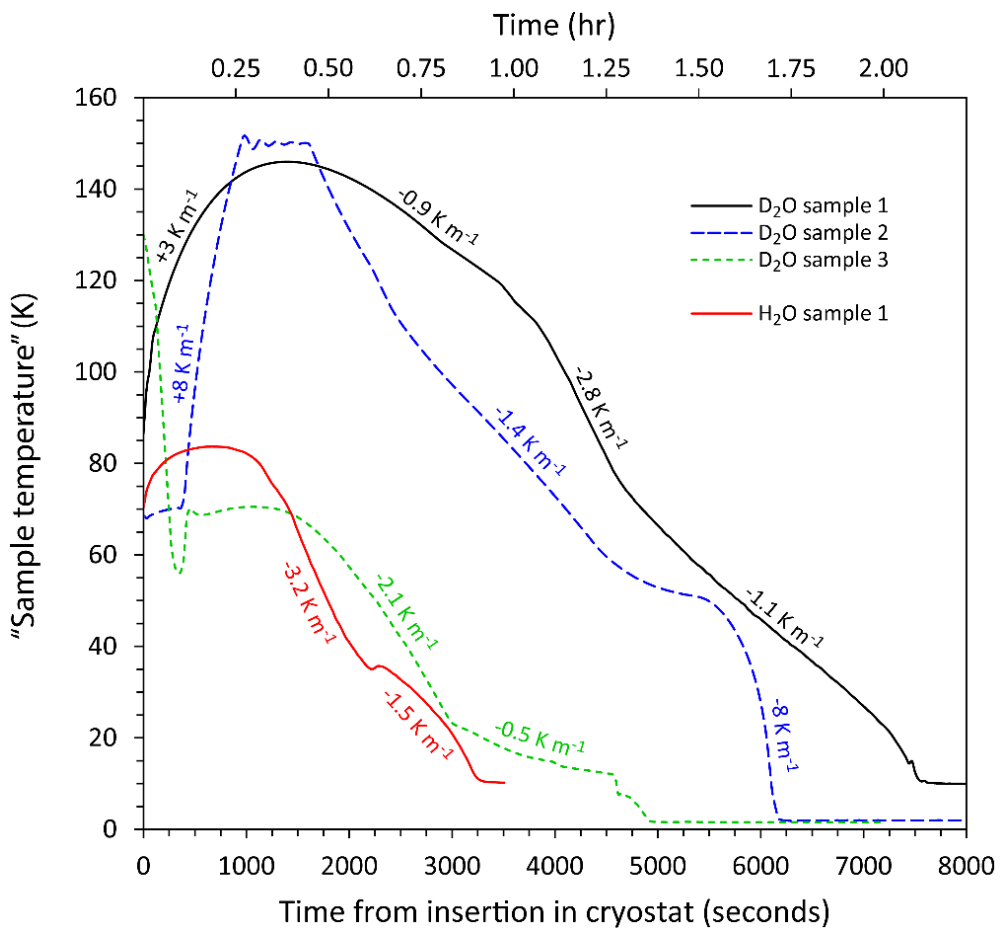


Figure S13: Plot of the logged sample temperatures after insertion in the cryostat. Variations in cooling rates reflect manual adjustments in exchange-gas pressure (CCR) or helium flow rates (“Orange” cryostat) as well as the intrinsic variations in the sample holder’s heat capacity.

# Electronic Supplementary Text and Figures

Table S1: Lattice parameters of H<sub>2</sub>O ice Ih as a function of temperature.

H <sub>2</sub> O series 1			H <sub>2</sub> O series 2		
T (K)	a (Å)	c (Å)	T (K)	a (Å)	c (Å)
9.94(2)	4.49679(3)	7.32208(10)	1.559(3)	4.49678(3)	7.32192(7)
19.94(3)	4.49668(3)	7.32188(10)	4.99(4)	4.49679(3)	7.32191(8)
30.08(3)	4.49648(3)	7.32181(10)	14.97(4)	4.49675(3)	7.32200(8)
40.09(2)	4.49636(3)	7.32124(10)	25.03(4)	4.49662(3)	7.32182(9)
49.98(1)	4.49611(3)	7.32127(11)	34.95(2)	4.49642(3)	7.32136(8)
60.06(1)	4.49615(3)	7.32091(10)	45.01(1)	4.49627(3)	7.32102(9)
70.00(1)	4.49615(3)	7.32105(11)	54.97(1)	4.49617(3)	7.32094(9)
79.97(2)	4.49640(4)	7.32130(11)	64.98(1)	4.49621(3)	7.32081(9)
90.02(1)	4.49676(4)	7.32170(12)	75.03(1)	4.49629(3)	7.32107(9)
100.00(1)	4.49722(4)	7.32243(12)	84.95(1)	4.49660(3)	7.32139(9)
110.03(1)	4.49786(4)	7.32363(12)	95.00(1)	4.49703(3)	7.32220(9)
120.02(2)	4.49872(4)	7.32450(12)	102.04(1)	4.49743(3)	7.32281(10)
130.02(1)	4.49958(4)	7.32608(13)	103.99(1)	4.49757(3)	7.32294(9)
139.96(2)	4.50065(4)	7.32757(13)	106.03(3)	4.49765(3)	7.32308(10)
149.98(2)	4.50175(4)	7.32987(13)	107.98(1)	4.49783(3)	7.32304(10)
159.98(1)	4.50296(4)	7.33186(13)	110.03(1)	4.49795(3)	7.32339(10)
169.95(1)	4.50428(4)	7.33421(13)	111.97(1)	4.49810(3)	7.32348(10)
184.99(2)	4.50653(5)	7.33781(15)	114.01(2)	4.49829(3)	7.32365(9)
199.96(3)	4.50903(5)	7.34192(15)	116.05(2)	4.49842(3)	7.32399(10)
215.04(1)	4.51169(5)	7.34614(16)	117.99(1)	4.49855(3)	7.32410(10)
230.04(2)	4.51475(6)	7.35106(18)	120.02(1)	4.49874(3)	7.32450(10)
244.96(1)	4.51783(6)	7.35630(19)	121.97(1)	4.49888(4)	7.32472(10)
254.99(2)	4.52018(7)	7.35995(22)	124.00(2)	4.49903(4)	7.32504(10)
265.03(2)	4.52235(8)	7.36391(25)	126.03(1)	4.49923(4)	7.32543(11)
			127.98(1)	4.49942(4)	7.32571(10)
			130.01(2)	4.49963(4)	7.32605(10)

## Electronic Supplementary Text and Figures

Table S2: Lattice parameters of D<sub>2</sub>O ice Ih as a function of temperature.

D <sub>2</sub> O series 1			D <sub>2</sub> O series 2			D <sub>2</sub> O series 3		
T (K)	a (Å)	c (Å)	T (K)	a (Å)	c (Å)	T (K)	a (Å)	c (Å)
9.93(2)	4.497301(9)	7.324044(23)	1.99(2)	4.497366(8)	7.323872(22)	1.601(0)	4.497313(7)	7.324454(19)
12.02(2)	4.497293(10)	7.324017(24)	2.97(3)	4.497401(8)	7.323884(21)	5.00(4)	4.497313(10)	7.324465(26)
14.03(3)	4.497278(10)	7.324049(24)	4.98(3)	4.497393(8)	7.323892(22)	10.02(4)	4.497310(10)	7.324478(26)
15.94(2)	4.497282(9)	7.323976(24)	6.97(2)	4.497389(8)	7.323902(22)	14.97(6)	4.497294(10)	7.324435(26)
17.91(2)	4.497259(10)	7.323919(25)	9.02(2)	4.497403(8)	7.323854(22)	20.04(5)	4.497210(10)	7.324279(27)
19.95(3)	4.497233(9)	7.323902(23)	9.98(5)	4.497388(8)	7.323901(22)	24.89(3)	4.497124(10)	7.324183(28)
22.12(2)	4.497200(9)	7.323896(23)	11.03(2)	4.497396(8)	7.323913(21)	29.99(2)	4.497028(10)	7.323956(26)
23.97(2)	4.497170(9)	7.323865(24)	12.99(5)	4.497392(8)	7.323868(21)	35.03(4)	4.496918(10)	7.323822(26)
26.12(2)	4.497122(9)	7.323777(24)	15.05(2)	4.497386(8)	7.323835(22)	39.95(3)	4.496831(10)	7.323679(26)
27.99(3)	4.497104(9)	7.323749(24)	16.91(2)	4.497370(8)	7.323837(21)	45.00(4)	4.496739(10)	7.323486(27)
30.08(3)	4.497055(9)	7.323601(25)	19.02(2)	4.497343(8)	7.323809(21)	50.06(3)	4.496681(10)	7.323379(27)
31.87(2)	4.497021(9)	7.323606(24)	21.06(2)	4.497313(8)	7.323768(22)	54.98(4)	4.496621(10)	7.323297(26)
34.00(3)	4.496973(9)	7.323554(24)	23.08(1)	4.497280(8)	7.323718(22)	60.04(5)	4.496615(11)	7.323256(27)
35.91(3)	4.496929(9)	7.323444(24)	24.99(2)	4.497244(8)	7.323630(22)	65.02(5)	4.496657(10)	7.323242(27)
38.06(1)	4.496918(9)	7.323378(24)	27.42(2)	4.497218(8)	7.323583(21)	70.02(4)	4.496719(10)	7.323364(27)
40.08(2)	4.496865(9)	7.323296(24)	32.56(2)	4.497099(8)	7.323431(22)	75.03(5)	4.496795(10)	7.323551(28)
45.00(2)	4.496786(10)	7.323184(25)	37.55(1)	4.497005(8)	7.323196(22)	80.00(3)	4.496949(10)	7.323706(27)
49.97(2)	4.496712(9)	7.323040(25)	42.54(1)	4.496889(8)	7.323049(22)	85.05(1)	4.497143(10)	7.324027(27)
54.97(1)	4.496673(10)	7.322959(25)	47.57(2)	4.496820(9)	7.322874(23)	90.00(1)	4.497328(11)	7.324327(28)
60.07(2)	4.496664(10)	7.322890(26)	52.45(1)	4.496771(8)	7.322812(22)	95.019(6)	4.497593(11)	7.324693(29)
64.98(1)	4.496671(10)	7.322955(26)	57.54(1)	4.496741(9)	7.322756(23)	100.04(1)	4.497910(11)	7.325113(28)
70.02(2)	4.496726(10)	7.322978(25)	62.49(1)	4.496741(9)	7.322779(23)	101.986(3)	4.498025(12)	7.325303(31)
75.03(1)	4.496804(10)	7.323129(26)	67.56(1)	4.496796(9)	7.322800(24)	104.019(4)	4.498158(11)	7.325522(29)

## Electronic Supplementary Text and Figures

79.97(1)	4.496927(10)	7.323324(27)	72.51(1)	4.496887(9)	7.322870(23)	105.96(1)	4.498288(11)	7.325777(28)
84.95(1)	4.497092(10)	7.323575(26)	77.52(1)	4.496981(9)	7.323077(24)	108.00(1)	4.498459(11)	7.325950(29)
90.02(2)	4.497304(11)	7.323836(28)	82.46(1)	4.497143(9)	7.323339(24)	110.04(1)	4.498602(11)	7.326186(28)
95.00(2)	4.497560(10)	7.324199(27)	87.47(1)	4.497341(9)	7.323647(24)	111.965(5)	4.498750(11)	7.326408(30)
100.00(2)	4.497848(10)	7.324656(27)	91.995(7)	4.497554(9)	7.323926(24)	114.01(1)	4.498917(11)	7.326657(30)
110.04(1)	4.498515(11)	7.325694(29)	93.999(7)	4.497658(9)	7.324066(25)	116.04(1)	4.499080(12)	7.326945(30)
120.03(1)	4.499362(12)	7.326998(31)	95.996(8)	4.497758(9)	7.324208(24)	117.98(1)	4.499267(11)	7.327220(29)
130.02(2)	4.500374(12)	7.328481(34)	97.974(5)	4.497854(9)	7.324323(24)	120.01(1)	4.499446(11)	7.327530(29)
139.96(3)	4.501466(13)	7.330281(35)	99.995(4)	4.497970(9)	7.324516(25)	121.954(6)	4.499615(11)	7.327808(29)
149.98(4)	4.502739(12)	7.332327(32)	101.957(4)	4.498105(9)	7.324729(25)	123.991(5)	4.499798(12)	7.328119(32)
159.98(2)	4.504151(12)	7.334461(32)	104.012(4)	4.498227(9)	7.324927(25)	126.02(1)	4.500004(11)	7.328452(30)
169.95(1)	4.505642(13)	7.336908(34)	105.968(5)	4.498390(9)	7.325113(25)	127.97(2)	4.500290(12)	7.328795(31)
180.00(1)	4.507303(13)	7.339648(35)	108.01(2)	4.498501(9)	7.325367(25)	130.00(2)	4.500506(11)	7.329063(30)
190.01(1)	4.509088(13)	7.342526(36)	109.96(1)	4.498655(9)	7.325612(25)	140.00(7)	4.501665(12)	7.330888(31)
199.96(1)	4.510977(14)	7.345711(38)	111.998(5)	4.498825(9)	7.325885(25)	159.99(2)	4.504431(13)	7.334900(32)
209.98(1)	4.512887(14)	7.348732(39)	114.036(5)	4.498986(9)	7.326100(26)	179.99(3)	4.507680(14)	7.340247(36)
219.97(1)	4.515012(15)	7.352165(41)	115.976(3)	4.499158(9)	7.326353(26)	200.00(3)	4.511433(14)	7.346450(38)
230.05(1)	4.517319(15)	7.355829(39)	118.010(4)	4.499337(10)	7.326552(27)	220.02(3)	4.515627(15)	7.353185(40)
240.05(1)	4.519682(15)	7.359641(41)	120.045(5)	4.499539(10)	7.326831(26)	240.07(3)	4.520216(16)	7.360518(42)
249.97(1)	4.522151(15)	7.363602(44)	121.984(6)	4.499719(10)	7.327195(26)	260.02(3)	4.525293(18)	7.368502(46)
260.01(2)	4.524728(16)	7.367756(46)	124.02(1)	4.499909(10)	7.327463(27)	269.99(3)	4.527646(18)	7.372385(48)
269.96(1)	4.527401(17)	7.371856(50)	125.96(1)	4.500110(10)	7.327785(28)			
			128.000(6)	4.500305(10)	7.328114(27)			
			130.032(4)	4.500536(10)	7.328430(26)			

## Electronic Supplementary Text and Figures

Table S3: Historical and contemporary data on the density of H<sub>2</sub>O ice Ih at its melting point.

Specific gravity	Density (g cm <sup>-3</sup> )	Reference	Note
82 : 91½	~0.900	Boyle (1665)	
8 : 9	~0.888	Musschenbroek (1734)	
0.905	~0.905	Krafft (1746)	
11 : 12	~0.917	Mairan (1749)	
14 : 15	~0.937	Irving, reported by Phipps (1774)	
0.945	0.945	Williams (1790)	(1)
243 : 272	0.8934	Heinrich (1806)	(2)
87 : 95	0.9158	— " —	
120 : 131	0.9160	— " —	
0.885	0.885	Meineke (1815)	(3)
14 : 15	~0.937	Scoresby (1818)	
0.920 ‡	0.919	Thomson (1818)	
0.915–0.925	0.915–0.925	Scoresby (1820)	
0.950 †	0.950	Le Royer & Dumas (1821)	
0.9268 *	0.9267	Osann (1830)	
0.9184 *	0.9183	Playfair & Joule (1845)	
0.9180 *	0.9179	Brunner (1845)	
0.91580 *	0.91565	Plücker & Geißler (1852)	
0.9078 *	0.9077	Kopp (1855)	
0.9175(7) *	0.9174(7)	Dufour (1860)	
0.9178(5) *	0.9177(5)	Dufour (1862)	
0.918–0.922 †	0.918–0.922	Duvernoy (1870)	
0.91674 †	0.91674	Bunsen (1870)	
0.91686	0.91686	Petterson (1883)	
0.916660	0.916660	Zakrzewski (1892)	
0.91614(2) *	0.91599(2)	Nicholls (1899)	(4)
0.91615(9) *	0.91600(9)	— " —	(5)
0.91807(4) *	0.91792(4)	— " —	(5)
0.91661(7) *	0.91646(7)	Barnes (1901)	
—	0.9160	Vincent (1902)	
0.91599**	0.91599	Dewar (1903)	
0.9176 *	0.91745	Leduc (1906)	
—	0.9157	Endo (1925)	(6)
—	0.91671(5)	Ginnings & Corruccini (1947)	
—	0.91680(4)	Dantl & Gregora (1968)	
—	0.9178(2)	Alimova <i>et al.</i> (1987)	
—	0.9159(5)	'Thermodynamic value'	(7)
—	0.91658(7)	This work (by extrapolation)	

\* Relative to water at 0 °C

† Relative to water at 4 °C

## Electronic Supplementary Text and Figures

† Relative to water at 15.56 °C (specifically, 60 °F).

\*\*Reference water temperature not stated, assumed to be 4 °C.

- (1) The specific gravity is actually calculated and reported by Charles Hutton on the basis of other data given by Major Williams.
- (2) Reports a mean value of 75 : 83.
- (3) This cites Muschenbroek's value as 0.918, but questions whether this is referenced to the density of water at the correct temperature and calculates said correction.
- (4) Nichol's determination based on a literature survey.
- (5) Nichol's own values.
- (6) Calculated by me using data in Endo's paper.
- (7) calculated from  $dT_m/dP$  and  $\Delta S_m$  and  $\rho_{\text{water}}$ .

Some of the earlier density determinations are discussed by Dorsey (1940). Note that many of the widely reported values prior to around 1840 are of somewhat opaque origin; for example, numerous textbooks (such as Filcher's *Physikalisches Wörterbuch*, Berzelius' *Lehrbuch der Chemie*, or Kastner's *Grundriß der Experimentalphysik*) attribute a value of 0.916 to Musschenbroek, who gives the specific gravity as 8:9 (or 0.888) in several of his publications. Even Meineke (1815) states that Musschenbroek's value is 0.918 before going on to apply a correction for the inferred water temperature and then reporting a value of 0.885. There is no correction that can shift the specific gravity from 0.918 to 0.885 but it is not difficult to shift from 0.888 to 0.885. Comparatively few writers tabulate Musschenbroek's determination as 0.888 (examples include von Gerstner's *Handbuch der Mechanik* and Böttger's *Tabellarische der Specifischen Gewichte der Körper*).

# Electronic Supplementary Text and Figures

## 3. References cited in the Supplement

- Albinati, A., & Willis, B. T. M. (1982) The Rietveld method in neutron and X-ray powder diffraction. *J. Appl. Cryst.* **15**, 361–374.
- Alimova, I. A., Riskin, G. Ya., & Ushakova, T. A. (1987) Izotopniy effekt koeffitsiyentov ob'yemnogo teplovogo rasshireniya l'dov H<sub>2</sub>O i D<sub>2</sub>O (Изотопный эффект коеффициентов объемного теплового расширения льдов H<sub>2</sub>O и D<sub>2</sub>O) [Isotope effect on the coefficients of volume thermal expansion in H<sub>2</sub>O and D<sub>2</sub>O ice]. *Zh. Fiz. Khim.* **61**, 1063–1066 (in Russian).
- Amaya, A. J., Pathak, H., Modak, V. P., Laksmono, H., Loh, N. D., Sellberg, J. A., Sierra, R. G., McQueen, T. A., Hayes, M. J., Williams, G. J., Messerschmidt, M., Boutet, S., Bogan, M. J., Nilsson, A., Stan, C. A., & Wyslouzil, B. E. (2017) How cubic can ice be? *J. Phys. Chem. Lett.* **8**, 3216–3222.
- Aminoff, G. (1921) Über den Radius des Wasserstoffatoms in Kristallen. *Geologiska Föreningen I Stockholm Förhandlingar* **43**, 389–396.
- Anderson, C. E., & Ebenhack, D. G. (1965) Heavy water. In, *Analysis of Essential Nuclear Reactor Materials*, pp629–657. Aiken, S.C., USA.
- Andrews, T. (1886) Observations on pure ice and snow. *Proc. Royal Soc. London* **40**, 544–549.
- Arnold, O., & 27 co-authors (2014) Mantid—Data analysis and visualization package for neutron scattering and μSR experiments. *Nucl. Instrum. Methods Phys. Res. A*, **764**, 156–166.
- Barnes, H. T. (1901) On the density of ice. *Phys. Rev.* **13**, 55–59.
- Barnes, H. T., Hayward, J. W., & McLeod, N. M. (1914) The expansive force of ice. *Trans. Royal Soc. Canada, Series III*, **8** (section 3), 29–49.
- Barnes, W. H. (1929) The crystal structure of ice between 0° C and –183° C. *Proc. Royal Soc. London Ser. A*, **125**, 670–693.
- Bartholomé, E., & Clusius, K. (1935) Calorische messungen an schwerem Wasser. *Z. Phys. Chem. B* **28**, 167–177.
- Bass, R., Rossberg, D., & Ziegler, G. (1957) Die elastischen Konstanten des Eises. *Z. Phys.* **149**, 199–203.
- Batchelder, D. N., & Simmons, R. O. (1964) Lattice constants and thermal expansivities of silicon and of calcium fluoride between 6° and 322° K. *J. Chem. Phys.* **41**, 2324–2329.

## Electronic Supplementary Text and Figures

- Bennington, S. M., Li, J., Harris, M. J., & Ross, K. (1999) Phonon softening in ice Ih. *Physica B* **263–264**, 396–399.
- Beukel, A. van den. (1968) Specific heat of ice near the "ferroelectric" transition temperature. *Phys. Stat. Solidi* **28**, 565–568.
- Bjerrum, N. (1951) Structure and properties of ice I. The position of hydrogen atoms and the zero-point entropy of ice. *Kgl. Danske. Videnskab. Selskab. Math. Fys. Medd.* **27**, 3–56.
- Bjerrum, N. (1952) Structure and properties of ice. *Science* **115**, 385–390.
- Blackman, M., & Lisgarten, N. D. (1957) The cubic and other structural forms of ice at low temperatures and pressures. *Proc. Royal Soc. A* **239**, 93–107.
- Bogorodskii, V. V. (1964) Uprugije moduli kristalla l'da (Упругие модули кристалла льда) [The elastic moduli of crystalline ice]. *Akhust. Zh.* **10**, 152–155 (in Russian).
- Boyle, R. (1665) *New experiments and observations touching cold*. John Crook, London.
- Bragg, W. H. (1921) The crystal structure of ice. *Proc. Phys. Soc. London* **34**, 98–103.
- Bridgman, P. W. (1935) The pressure-volume-temperature relations of the liquid, and the phase-diagram of heavy water. *J. Chem. Phys.* **3**, 597–605.
- Brill, R., & Camp, P. R. (1961) Properties of ice. US Army Cold Regions Research and Engineering Laboratory. Research Report 68, 75pp.
- Brill, R., & Tippe, A. (1967) Gitterparameter von Eis I bei tiefen Temperaturen. *Acta Cryst.* **23**, 343–345.
- Brockamp, B., & Querforth, H. (1964) Untersuchung über die Elastizitätskonstanten von See- und Kunsteis. *Polarforsch.* **5**, 253–262.
- Brown, G. N., & Zielger, W. T. (1980) Vapor pressure and heats of vaporization and sublimation of liquids and solids of interest in cryogenics below 1-atm pressure. In *Advances in Cryogenic Engineering* (Timmerhaus, K. D., Ed), vol. 35A, pp. 662–670. Springer US.
- Brunner, C. (1845) Versuch über die Dichtigkeit des Eises bei verschiedenen Temperaturen. *Ann. Phys.* **64**, 113–124.
- Buckingham, D. T. W. (2017) *High-resolution thermal expansion and dielectric relaxation measurements of H<sub>2</sub>O and D<sub>2</sub>O ice Ih*. PhD Thesis, Montana State University.
- Buckingham, D. T. W., Masunaga, S. H., Gile, F. C., & Neumeier, J. J. (2014) High-resolution thermal expansion measurements of H<sub>2</sub>O ice. APS March Meeting 2014, abstract Y42.001

## Electronic Supplementary Text and Figures

- Buckingham, D. T. W., Masunaga, S. H., Gile, F. C., & Neumeier, J. J. (2015) Possible Phase Transition in H<sub>2</sub>O Ice Ih near 110 K. APS March Meeting 2015, abstract W12.007.
- Bunsen, R. (1870) Calorimetric untersuchungen. *Ann. Phys.* **141**, 1–30.
- Burton, E. F., & Oliver, W. F. (1935) The crystal structure of ice at low temperatures. *Proc. Royal Soc.* **153**, 166–172.
- Butkovich, T. (1959) Thermal expansion of ice. *J. Appl. Phys.* **30**, 350–353.
- Butkovich, T. R. (1955) Density of single crystals of ice from a temperate glacier. *J. Glaciol.* **2**, 553–559.
- Butkovich, T. R. (1957) Linear thermal expansion of ice. US Army Snow Ice and Permafrost Research Establishment. Research Report 40, 1–10.
- Camp, P. R. (1963) Properties of ice, part II. US Army Cold Regions Research and Engineering Laboratory. Research Report 114, 38pp.
- Chamberlain, J. S., & Fletcher, N. H. (1971) Low temperature polarization effects in ice. *Phys. Kond. Matt.* **12**, 193–209.
- Cochran, W. (1973) *The Dynamics of Atoms in Crystals*. Arnold, London.
- Dantl, G. (1962) Wärmeausdehnung von H<sub>2</sub>O- und D<sub>2</sub>O-Einkristallen. *Z. Phys.* **166**, 115–118.
- Dantl, G. (1968) Die elastischen Moduln von Eis-Einkristallen. *Phys. Kond. Mat.*, **7**, 390–397.
- Dantl, G., & Gregora, I. (1968) Dichte in hexagonalem eis. *Naturwiss.* **55**, 176–176.
- Dengel, O., Eckner, V., Plitz, H., & Riehl, N. (1964) Ferroelectric behaviour of ice. *Phys. Lett.* **9**, 291–292.
- Dennison, D. M. (1921) The crystal structure of ice. *Phys. Rev.* **17**, 20–22.
- Dewar, J. (1903) Low temperature investigations. *Proc. Royal Inst.* **17**, 418–426.
- Dorsey, N. E. (1940) *Properties of ordinary water substance*. New York. 673pp.
- Dufour, L. (1860) Sur la densité de la glace. *Comptes Rendus Acad. Sci. Paris* **50**, 1039–1040.
- Dufour, L. (1862) Sur la densité de la glace. *Comptes Rendus Acad. Sci. Paris* **54**, 1079–1082.
- Dumble, J. H. (1860) Some experiments on the expansion and contraction of ice. *Can. J. Ind. Sci. Art.* **5**, 418–426.
- Duvernoy, J. (1862) Ueber die Ausdehnung des Wassers beim Gerfrieren. *Ann. Phys. Ser. 2.* **117**, 454–463.

## Electronic Supplementary Text and Figures

- Endo, H. (1925) On the measurement of the change of volume in metals during solidification. *Sci. Rep. Tohoku Imp. Univ.* (1), **13**, 193–218.
- Ermolieff, A. (1975) Brillouin scattering in ice and deuterated ice as a function of temperature. *Solid State Comm.* **17**, 1013–1016.
- Fitzgerald, W. J., & O'Connor, D. A. (1976) Anomalies in the scattering of gamma-rays from single crystals of HF-doped ice-Ih around 100 K. *Z. Phys. B: Cond. Matt.* **24**, 1–5.
- Flubacher, P., Leadbetter, A. J., & Morrison, J. A. (1960) Heat capacity of ice at low temperatures. *J. Chem. Phys.* **33**, 1751–1755.
- Fortes, A. D., Wood, I. G., & Knight, K. S. (2008) The crystal structure and thermal expansion tensor of  $\text{MgSO}_4 \cdot 11\text{D}_2\text{O}$  (meridianiite) determined by neutron powder diffraction. *Phys. Chem. Min.* **35**, 207–221.
- Fortes, A. D., Wood, I. G., Grigoriev, D., Alfredsson, M., Kipfstuhl, S., Knight, K. S., & Smith, R. I. (2004) No evidence for large-scale proton ordering in Antarctic ice from neutron powder diffraction. *J. Chem. Phys.* **120**, 11376–11379.
- Fortes, A. D., Wood, I. G., Knight, K. S., Alfredsson, M., & Vočadlo, L. (2005) The incompressibility and thermal expansivity of  $\text{D}_2\text{O}$  ice II determined by neutron diffraction. *J. Appl. Cryst.* **38**(4), 612–618.
- Fortes, A. D., Wood, I. G., Knight, K. S., Alfredsson, M., & Vočadlo, L. (2006) The thermoelastic properties of epsomite ( $\text{MgSO}_4 \cdot 7\text{D}_2\text{O}$ ) from powder neutron diffraction and *ab initio* simulation. *Eur. J. Min.* **18**, 449–462.
- Fortes, A. D., Wood, I. G., Tucker, M. G., & Marshall, W. G. (2012) The P-V-T equation of state of  $\text{D}_2\text{O}$  ice VI determined by neutron powder diffraction in the range  $0 < P < 2.6$  GPa,  $120 < T < 330$  K, and the isothermal equation of state of  $\text{D}_2\text{O}$  ice VII from 2 to 7 GPa at room temperature. *J. Appl. Cryst.* **45**, 523–534.
- Fowler, R. H. (1934) The heavy isotope of hydrogen. The Liversedge Lecture, 1934. *Math. Proc. Camb. Phil. Soc.* **30**, 225–241.
- Fukusako, S. (1990) Thermophysical properties of ice, snow, and sea ice. *Int. J. Thermophys.* **11**, 353–372.
- Gagnon, R. E., Kieft, H., Clouter, M. J., & Whalley, E. (1987) Elastic constants of ice Ih, up to 2.8 kbar, by Brillouin spectroscopy. *J. de Phys. Coll.* **48**, C1,23–C1,28.
- Gammon, P. H., Kieft, H., & Clouter, M. J. (1980) Elastic constants of ice samples by Brillouin spectroscopy. *J. Glaciol.* **25**, 159–167.

## Electronic Supplementary Text and Figures

- Gammon, P. H., Kieft, H., & Clouter, M. J. (1983a) Elastic constants of ice samples by Brillouin spectroscopy. *J. Phys. Chem.* **87**, 4025–4029.
- Gammon, P. H., Kieft, H., Clouter, M. J., & W. W. Denner (1983b) Elastic constants of artificial and natural ice samples by Brillouin spectroscopy. *J. Glaciol.* **29**, 433–460.
- Geil, B., Kirschgen, T. M., & Fujara, F. (2005) Mechanism of proton transport in hexagonal ice. *Phys. Rev. B* **72**, article 014304.
- Giauque, W. F., & Stout, J. W. (1936) The entropy of water and the third law of thermodynamics. The heat capacity of ice from 15 to 273 °K. *J. Am. Chem. Soc.* **58**, 1144–1150.
- Gillet, P., Richet, P., Guyot, F., & Fiquet, G. (1991) High-temperature thermodynamic properties of forsterite. *J. Geophys. Res.: Solid Earth* **96**, 11805–11816.
- Ginnings, D. C., & Corruccini, R. J. (1947) An improved ice calorimeter – the determination of its calibration factor and density of ice at 0° C. *J. Res. Natl. Bur. St.* **38**, 583–591.
- Glassenbrenner, C. J., & Slack, G. A. (1964) Thermal conductivity of silicon and germanium from 3 °K to the melting point. *Phys. Rev.* **134**, A1058–A1069.
- Gränicher, H. (1958) Lattice disorder and physical properties connected with the hydrogen arrangement in ice crystals. *Proc. Royal Soc. London A* **247**, 453–461.
- Green, R. F., & Mackinnon, L. (1955) Determination of the elastic constants of ice single crystals by an ultrasonic pulse method. *J. Acoust. Soc. America* **28**, 1292–1292.
- Grishina, N., & Buch, V. (2004) Structure and dynamics of orientational defects in ice I. *J. Chem. Phys.* **120**, 5217–5225.
- Gross, R. (1919) Das Lauephotogramm des Eises. *Centralblatt für Mineralogie, Geologie und Paläontologie*, **1919**, 201–207.
- Grüneisen, E. (1912) Theorie des festens Zustandes einatomiger Element. *Ann. Phys.* **12**, 257–306.
- Haida, O. (1979) Enthalpy relaxation phenomenon of heavy ice. *J. Glaciol.* **22**, 155–164.
- Haida, O., Matsuo, T., Suga, H., & Seki, S. (1974) Calorimetric study of the glassy state. X. Enthalpy relaxation at the glass-transition temperature of hexagonal ice. *J. Chem. Thermodyn.* **6**, 815–825.
- Haida, O., Suga, H., & Seki, S. (1973) Enthalpy relaxation at glass transition temperature of heavy ice crystal. *Proc. Jap. Acad.* **49**, 191–195.

## Electronic Supplementary Text and Figures

- Haltenorth, H. (1974) *Messung des Debye-Waller-Faktors und des Gitterparameters a an H<sub>2</sub>O-Eis-Ih-Einkristallen zwischen 90 Grad und 230 Grad Kelvin.* Thesis, Technische Universität München.
- Hansen, T. C., Koza, M. M., & Kuhs, W. F. (2008) Formation and annealing of cubic ice: I. Modelling of stacking faults. *J. Phys.: Cond. Matt.* **20**, article 285104.
- Hansen, T. C., Sippel, C., & Kuhs, W. F. (2015) Approximations to the full description of stacking disorder in ice I for powder diffraction. *Z. Krist.* **230**, 75–86.
- Heinrich, P. (1806) Pyrometrisches Versuche über die Ausdehnung des Eises und der Holzkohle. *Phys. Abh. königlich-baierischen Akad. Wiss.* **1802-1805**. 2<sup>te</sup> abt., 149–200.
- Helmreich, D., & Bullemer, B. (1969) Anomales elastisches Verhalten von Eis bei tiefen Temperaturen. *Phys. Kond. Matt.* **8**, 384–392.
- Henderson, S. J., & Speedy, R. J. (1987) Melting temperature of ice at positive and negative pressures. *J. Phys. Chem.* **91**, 3069–3072.
- Hoffmeister, A. M. (2014) Thermal diffusivity and thermal conductivity of single-crystal MgO and Al<sub>2</sub>O<sub>3</sub> and related compounds as a function of temperature. *Phys. Chem. Min.* **41**, 361–371.
- Hondoh, T. (2015) Dislocation mechanism for transformation between cubic ice Ic and hexagonal ice Ih. *Phil. Mag.* **95**, 3590–3620.
- Ibberson, R.M. (2009) Design and performance of the new supermirror guide on HRPD at ISIS. *Nuclear Instruments and Methods in Physics Research A* **600**, 47–49.
- Ibberson, R.M., David, W.I.F., and Knight, K.S. (1992) The high resolution neutron powder diffractometer (HRPD) at ISIS – a user guide. RAL-92-031. Rutherford Appleton Laboratory, U. K. (<http://www.isis.rl.ac.uk/crystallography/documentation/HRPDguide>).
- Irving, C. (1774) In, Phipps, C. J., *A Voyage towards the North Pole, undertaken by his Majesty's Command.* London.
- Jakob, M., & Erk, S. (1929) Wärmedehnung des Eises zwischen 0 und -253°. *Wiss. Abhandl. Phys. Tech. Reichsanstalt* **12**, 302–316.
- Jeneveau, A., & Sixou, P. (1972) Dipolar relaxation at low temperature of ice single crystal. *Solid State Comm.* **10**, 191–194.
- Jeneveau, A., Sixou, P., & Dansas, P. (1972) Etude du comportement électrique de la glace pure en basse température — ferroélectricité et charge d'espace. *Phys. Kond. Mat.* **14**, 252–264.

## Electronic Supplementary Text and Figures

- Johari, G. P., & Jones, S. J. (1975) Study of the low-temperature "transition" in ice Ih by thermally stimulated depolarization measurements. *J. Chem. Phys.* **62**, 4213–4223.
- Johari, G. P., & Jones, S. J. (1976) Dielectric properties of polycrystalline D<sub>2</sub>O ice Ih (hexagonal). *Proc. Royal Soc. London A* **349**, 467–495.
- Jona, F., & Scherrer, P. (1952) Die elastischen Konstanten von Eisenkristallen. *Helv. Phys. Acta* **25**, 35–54.
- Khamzin, A. A., & Nigmatullin, R. R. (2017) Multiple-trapping model of dielectric relaxation of the ice Ih. *J. Chem. Phys.* **147**, article 204502.
- Klinger, J., & Rochas, O. (1982) Anisotropic heat conduction of fresh hexagonal ice single crystals at low temperature. *J. Phys. C: Solid State Phys.* **15**, 4503–4509.
- Klotz, S., Komatsu, K., Kagi, H., Kunc, K., Sano-Furukawa, A., Machida, S., & Hattori, T. (2017) Bulk moduli and equations of state of ice VII and VIII. *Phys. Rev. B* **95**, article 174111.
- Kobayashi, K., & Yasuda, H. (2012) Phase transition of ice Ic to ice XI under electron beam irradiation. *Chem. Phys. Lett.* **547**, 9–12.
- Kohl, I., Mayer, E., & Hallbrucker, A. (2000) The glassy water–cubic ice system: a comparative study by X-ray diffraction and differential scanning calorimetry. *Phys. Chem. Chem. Phys.* **2**, 1579–1586.
- Kopp, H. (1855) Ueber die Volumänderung einiger Substanzen beim Erwärmen und Schmelzen. *Ann. Chem. Pharm.* **93**, 129–232.
- Krafft, G. W. (1746) De Calore ac Frigore Experimenta Varia. *Comm. Acad. Sci. Imp. Petropol.* **14**, 218–239.
- Kuhs, W. F., Sippel, C., Falenty, A., & Hansen, T. C. (2012) Extent and relevance of stacking disorder in “ice Ic”. *Proc. Natl. Acad. Sci.* **109**, 21259–21264.
- Kumai, M. (1967) A study of hexagonal and cubic ice at low temperatures. US Army Cold Regions Research and Engineering Laboratory. Research Report 231, 17pp.
- LaPlaca, S., & Post, S. (1960) Thermal expansion of ice. *Acta Cryst.* **13**, 503–505.
- Larson, A.C. & Von Dreele, R.B. (1994) *General Structure Analysis System (GSAS)*. Los Alamos National Laboratory Report, LAUR 86-748.
- Le Bail, A. (2005) Whole powder pattern decomposition methods and applications: A retrospection. *Powder Diff.* **20**, 316–326.
- Le Royer, M. A. & Dumas, J. –A. (1821) Essai sur le volume de l’atome des corps. *J. Phys. Chim. Hist. Nat.* **42**, 401–411.

## Electronic Supplementary Text and Figures

- Leadbetter, A. J. (1965) The thermodynamic and vibrational properties of H<sub>2</sub>O and D<sub>2</sub>O ice. *Proc. Royal Soc. London A: Math. Phys. Sci.* **287**, 403–425.
- Leduc, A. (1906) Sur la densité de la glace. *Comptes Rendus Acad. Sci. Paris* **142**, 149–151.
- Li, J. (1996) Inelastic neutron scattering studies of hydrogen bonding in ices. *J. Chem. Phys.* **105**, 6733–6755.
- Line, C. M., & Whitworth, R. W. (1996) A high resolution neutron powder diffraction study of D<sub>2</sub>O ice XI. *J. Chem. Phys.* **104**, 10008–10013.
- Long, E. A., & Kemp, J. D. (1936) The entropy of deuterium oxide and the third law of thermodynamics. Heat capacity of deuterium oxide from 15 to 298°K. The melting point and heat of fusion. *J. Am. Chem. Soc.* **58**, 1829–1834.
- Lonsdale, K. (1958) The structure of ice. *Proc. Royal. Soc. A* **247**, 424–434.
- Lyon, K. G., Salinger, G. L., Swenson, C. A., & White, G. K. (1977) Linear thermal expansion measurements on silicon from 6 to 340 K. *J. Appl. Phys.* **48**, 865–868.
- Mairan, J. J. D. de (1749) *Dissertation sur la glace*. Leipzig.
- Malkin, T. L., Murray, B. J., Brukhno, A. V., Anwar, J., & Salzmann, C. G. (2012) Structure of ice crystallized from supercooled water. *Proc. Natl. Acad. Sci.* **109**, 1041–1045.
- Malkin, T. L., Murray, B. J., Salzmann, C. G., Molinero, V., Pickering, S. J., & Whale, T. F. (2015) Stacking disorder in ice I. *Phys. Chem. Chem. Phys.* **17**, 60–76.
- Mantid (2013) Manipulation and Analysis Toolkit for Instrument Data; Mantid Project. <http://dx.doi.org/10.5286/SOFTWARE/MANTID>.
- Marchand, R. F. (1845) Ueber die Dichtigkeit des Eises bei verschiedenen Temperaturen. *J. Prakt. Chem.* **35**, 254–256.
- Megaw, H. D. (1934) Cell dimensions of ordinary and heavy ice. *Nature* **134**, 900–901.
- Meineke, J. L. G. (1815) *Die chemische Meßkunst oder Anleitung, die chemischen Verbindungen nach Maaß und Gewicht auf eine einfache Weise zu bestimmen und zu berechnen, auf Versuche gegründet und durch Beispiele erläutert*. Halle und Leipzig. 279pp.
- Mitzdorf, U., & Helmreich, D. (1971) Elastic constants of D<sub>2</sub>O ice and variation of intermolecular forces on deuteration. *J. Acoust. Soc. America* **49**, 723–728.
- Moritz, A., & Pohrt, U. W. (1848) Der Ausdehnungs-coefficient des Eises. *Extrait des Mémoires de l'Académie VI Serie., Sciences, Mathématiques et Physics.* **4**, 64–90.
- Moseley, H. (1870) On the mechanical properties of ice. *Phil. Mag. 4<sup>th</sup> Series*, **39**, 1–8.

## Electronic Supplementary Text and Figures

- Murray, B. J., Knopf, D. A., & Bertram, A. K. (2005) The formation of cubic ice under conditions relevant to Earth's atmosphere. *Nature* **434**, 202–205.
- Murray, É. D., & Galli, G. (2012) Dispersion interactions and vibrational effects in ice as a function of pressure: a first principles study. *Phys. Rev. Lett.* **108**, article 105502.
- Musschenbroek, P. von (1734) *Elementa Physicae conscripta in usus ad academicos*. Leyden.
- Neumeier, J. J., Bollinger, R. K., Timmins, R. K., Lane, C. R., Krogstad, R. D., & Macaluso, J. (2008) Capacitive-based dilatometer cell constructed of fused quartz for measuring the thermal expansion of solids. *Rev. Sci. Instr.* **79**, article 033903.
- Nicholls, E. L. (1899) On the density of ice. *Phys. Rev.* **8**, 21–37.
- Northwood, T. D. (1947) Sonic determination of the elastic properties of ice. *Can. J. Res.* **25A**, 88–95.
- Okada, Y., & Tokumaru, Y. (1984) Precise determination of lattice parameter and thermal expansion coefficients of silicon between 300 and 1500 K. *J. Appl. Phys.* **56**, 314–320.
- Osann, G. (1830) Ueber das Eigengewicht des Eises. *Archiv Ges. Natur.* **19**, 95–100.
- Owston, P. G. (1958) The structure of ice-I, as determined by x-ray and neutron diffraction analysis. *Adv. Phys.* **7**, 171–188.
- Pamuk, B., Sohler, J. M., Ramírez, R., Herrero, C. P., Stephens, P. W., Allen, P. B., & Fernández-Serra, M. –V. (2012) Anomalous nuclear quantum effects in ice. *Phys. Rev. Lett.* **108**, article 193003.
- Peterson, S. W., & Levy, H. A. (1957) A single-crystal neutron diffraction study of heavy ice. *Acta Cryst.* **10**, 70–76.
- Pettersson, O. (1883) On the properties of water and ice. In, Nordenskjold, A. E., ed. *Vega-expeditionens vetenskapliga iakttagelser*. Bd. 2. Stockholm, F. and G. Beijers Forlag, 247–323.
- Playfair, L., & Joule, J. P. (1845) On atomic volume and specific gravity. *London, Edinb. Dublin Phil. Mag. J. Sci.* **27**, 453–533.
- Plücker, J. & Geißler, H (1852) Studien über Thermometrie und verwandte Gegenstände. *Ann. Phys.* **86**, 238–279.
- Podeszwa, R., & Buch, V. (1999) Structure and dynamics of orientational defects in ice. *Phys. Rev. Lett.* **83**, 4570–4573.
- Popov, I., Lunev, I., Khamzin, A., Greenbaum, A., Gusev, Y., & Feldman, Y. (2017) The low-temperature dynamic crossover in the dielectric relaxation of ice Ih. *Phys. Chem. Chem. Phys.* **19**, 28610–28620.

## Electronic Supplementary Text and Figures

- Popov, I., Puzenko, A., Khamzin, A., & Feldman, Y. (2015) The dynamic crossover in dielectric relaxation behavior of ice Ih. *Phys. Chem. Chem. Phys.* **17**, 1489–1497.
- Powell, R. W. (1958) Preliminary measurements of the thermal conductivity and expansion of ice. *Proc. Royal Soc. London A: Math. Phys. Sci.* **247**, 464–466.
- Proctor, T. M. (1966) Low temperature speed of sound in single-crystal ice. *J. Acoust. Soc. America* **39**, 972–977.
- Rinne, F. (1917) Das kristallsystem und das Achsenverhältnis des Eises. *Ber. Verhandl. Königl. Sächs. Ges. Wiss.* **69**, 57–62.
- Röttger, K., Endris, A., Ihringer, J., Doyle, S., & Kuhs, W. F. (1994) Lattice constants and thermal expansion of H<sub>2</sub>O and D<sub>2</sub>O ice Ih between 10 and 265 K. *Acta Cryst. B* **50**, 644–648.
- Röttger, K., Endris, A., Ihringer, J., Doyle, S., & Kuhs, W. F. (2012) Lattice constants and thermal expansion of H<sub>2</sub>O and D<sub>2</sub>O ice Ih between 10 and 265 K. Addendum. *Acta Cryst. B* **68**, 91.
- Sakatume, S., & Seki, N. (1978) Tei ondo-iki ni okeru kōri oyobi yuki no netsu tokusei (低温度域における氷および雪の熱特性) [Thermal properties of ice and snow in a low temperature range]. *Trans. Japan Soc. Mech. Eng.* **44**, 2059–2069 (in Japanese).
- Salim, M. A., Willow, S. Y., & Hirata, S. (2016) Ice Ih anomalies: thermal contraction, anomalous volume isotope effect, and pressure-induced amorphization. *J. Chem. Phys.* **144**, article 204503.
- Sasaki, K., Kita, R., Shinyashiki, N., & Yagihara, S. (2016) Dielectric relaxation time of ice-Ih with different preparation. *J. Phys. Chem. B* **120**, 3950–3953.
- Sawyer, W. H. (1911) Observations and experiments on ice expansion. *Proc. Maine Soc. Civil Eng.* **1**, 27–40.
- Schumacher, C. A. (1848) Versuche über die ausdehnung des eises. *Extrait des Mémoires de l'Académie VI Serie., Sciences, Mathématiques et Physics.* **4**, 13–63.
- Scoresby, W. (1818) On the Greenland or Polar Ice. *Mem. Wernerian Natl. Hist. Soc Edinburgh. Part II.*, **2**, 261–388.
- Scoresby, W. (1820) *An Account of the Arctic regions with history and description of the northern whale-fishery*. Edinburgh.
- Sears, V. F. (1992) Neutron scattering lengths and cross sections. *Neutron News* **3**, 26–37.  
<https://www.ncnr.nist.gov/resources/n-lengths/>
- Slack, G. A. (1980) Thermal conductivity of ice. *Phys. Rev. B* **22**, 3065–3071.

## Electronic Supplementary Text and Figures

- Slater, J. C. (1939) *Introduction to Chemical Physics*. McGraw-Hill, New York.
- Smirnova, N. N., Bykova, T. A., Van Durme, K., & Van Mele, B. (2006) Thermodynamic properties of deuterium oxide in the temperature range from 6 to 350 K. *J. Chem. Thermodyn.* **38**, 879–883.
- St. John., A. (1918) The crystal structure of ice. *Proc. Natl. Acad. Sci. USA* **4**, 193–197.
- Strässle, Th., Saitta, A. M., Klotz, S., & Braden, M. (2004) Phonon dispersion of ice under pressure. *Phys. Rev. Lett.* **93**, article 225901.
- Struve, W. (1848) Sur la dilatation de la glace d'après les expériences faites en 1845 et 1846 à l'observatoire central de Pulkovo, par MM. Schumacher, Pohrt et Moritz. *Extrait des Mémoires de l'Académie VI Serie., Sciences, Mathématiques et Physics.* **4**, 1–12.
- Sugisaki, M., Suga, H., & Seki, S. (1968) Calorimetric study of the glassy state. IV. Heat capacities of glassy water and cubic ice. *Bull. Chem. Soc. Japan* **41**, 2591–2599.
- Thomson, T. (1818) *System of Chemistry*, Vol. 1. Philadelphia (p 514).
- Toby, B.H. (2001) EXPGUI, a graphical user interface for GSAS. *J. Appl. Crystallogr.* **34**, 210–213.
- Tonkonogov, M. P. (1998) Dielectric spectroscopy of hydrogen-bonded crystals, and proton relaxation. *Phys. Usp.* **41**, 25–48.
- Truby, F. K. (1955) Lattice constants of pure and fluoride-contaminated ice. *Science* **121**, 404–404.
- Umemoto, K., & Wentzcovich, R. M. (2017) First principles study of volume isotope effects in ices VIII and X. *Japan. J. Appl. Phys.* **56**, article 05FA03.
- Umemoto, K., Sugimura, E., de Gironcoli, S., Nakajima, Y., Hirose, K., Ohishi, Y., & Wentzcovich, R. (2015) Nature of the volume isotope effect in ice. *Phys. Rev. Lett.* **115**, article 173005.
- Uritski, A., Presiado, I., Erez, Y., Gepshtain, R., & Huppert, D. (2009) Temperature dependence of proton diffusion in Ih ice. *J. Phys. Chem. C* **113**, 10285–10296.
- Vedamuthu, M., Singh, S., & Wilse Robinson, G. (1994) Accurate mixture-model densities for D<sub>2</sub>O. *J. Phys. Chem.* **98**, 8591–8593.
- Vegard, L., & Hillesund, S. (1942) Die strukturen einiger deuterium verbindungen und ihr vergleich mit denjenigen der entsprechenden wasserstoffverbindungen. *Avh. Norske Videnskaps-Akademie Oslo., Mat. Natur. Klasse* **8**, 1–24.
- Vincent, J. H. (1902) On the density and cubical expansion of ice. *Proc. Royal. Soc. London* **198**, 463–481.

## Electronic Supplementary Text and Figures

- Wachtman, J. B., Tefft, W. E., Lamb, D. G., & Apstein, C. S. (1961) Exponential temperature dependence of Young's Modulus for several oxides. *Phys. Rev.* **122**, 1754–1759.
- Wagner, W., & Pruß, A. (2002) The IAPWS formulation 1995 for the thermodynamic properties of ordinary water substance for general and scientific use. *J. Phys. Chem. Ref. Data* **31**, 387–535.
- Wang, K. –T., & Brewster, M. Q. (2010) An intermolecular vibration model for lattice ice. *Int. J. Thermodyn.* **13**, 51–57.
- Williams, E. (1790) Experiments on the expansive force of freezing water. *Trans. Royal Soc. Edinburgh* **2**, 23–28.
- Wollan, E. O., Davidson, W. L., & Shull, C. G. (1949) Neutron diffraction study of the structure of ice. *Phys. Rev.* **75**, 1348–1352.
- Zakrzewski, J. von (1892) Ueber das specifische Gewicht und die Schmelzwärme des Eises. *Ann. Phys.* **47**, 155–162.
- Zarembowitch, A., & Kahane, A. (1964) Détermination des vitesses de propagation d'ondes ultrasonores longitudinales dans la glace. Étude de leur variation avec la température. *Comptes Rendus Acad. Sci. Paris* **58**, 2529–2532.